SUPPLEMENTARY INFORMATION

Supplementary Text

Further analysis of MTSEA blockade.

MTSEA blockade of G98C E106D Orai1 channels in Ca^{2+}-containing solutions occurred at a slow rate of only ~10^2 $M^{-1}s^{-1}$ **(Supplementary Fig. 1a)**, two orders of magnitude slower than the reaction of MTSEA with residues D110C and Q108C in the outer vestibule of Orai1 (~10^4 $M^{-1}s^{-1}$) [1], and significantly slower than the reaction rate of MTSEA with free thiols in solution [2]. When applied in a divalent free (DVF) solution, however, the rate of MTSEA block became significantly faster (~10^4 $M^{-1}s^{-1}$) **(Supplementary Fig. 1a)**, approaching rates seen for residues in the outer vestibule of Orai1 [1], indicating that flux of monovalent MTSEA ions in the CRAC channel pore is dramatically slowed in the presence of Ca^{2+}, analogous to the diminished flux of Na^+ ions by extracellular Ca^{2+} in native CRAC channels [3].

Analysis of subunit stoichiometry of V102A mutant Orai1 channels.

One explanation for the different ion selectivity of STIM1-bound and -free V102 mutant channels is the possibility that these channels have different subunit stoichiometries as proposed in a recent model [4]. Because STIM1-free Orai complexes are dimers in this model, the inevitable change in pore structure resulting from STIM1-induced assembly of dimers to tetramers could naturally lead to very different permeation properties [4]. We tested this possibility through the use of Cd^{2+}, a thiol-reagent that potently blocks currents in Orai1 channels bearing cysteine mutations at pore-lining positions [1]. Tight blockade by Cd^{2+} requires coordination of the ion by three or more pore-lining Cys residues [5,6] and we used this property to determine how many pore-

lining cysteines are present in the constitutively active V102A mutant. As outlined in **Supplementary Fig 8a**, we varied the number of cysteines in the assembled channel at D110, a Cd^{2+} sensitive position in the outer vestibule [1], by generating concatenated dimers with D110C substitutions in either both protomers or only one protomer **(Supplementary Fig. 8b)**. Because STIM1-bound Orai1 channels are tetrameric [4,7,8], the assembly of these Orai1 dimers in STIM1-expressing cells would produce channels with either four or two pore-lining cysteines. We found that in channels arising from STIM1-free V102A D110C Orai1 dimers, Cd^{2+} blockade was robust, largely irreversible and comparable to the block seen in the presence of STIM1 (**Supplementary Fig. 8a,c**). Importantly, this block was significantly larger than the 25±1.5% block seen in STIM1-bound channels with only one D110C substitution in the Orai1 dimer **(Supplementary Fig. 8a)**. These results are inconsistent with the presence of only two cysteines at D110 in the STIM1-free V102A Orai1 channels. Thus, a change in the stoichiometry of mutant STIM1-free channels is unlikely, arguing that the distinct permeation properties of STIM1-bound and -free V102A mutant channels are due to different pore structures of fully assembled, tetrameric channels.

While this manuscript was under review at Nature, Srikanth et al, reported that Cys mutation of W176 Orai1 located at the cytoplasmic rim of the third transmembrane domain (TM3) caused alterations in ion selectivity of Orai1 channels and also resulted in constitutive channel activation in the absence of STIM1 [9]. Because the available evidence shows that TM3 does not line the pore, these intriguing effects are likely due to destabilization of the selectivity filter and the channel gate through long-distance allosteric effects. They point to an interesting role for TM3 in stabilizing the pore-flanking TM1 segment, possibly through packing interactions. More studies are needed to address this possibility.

Supplementary Methods

$[Ca^{2+}]_i$ imaging. HEK293 cells plated on coverslips were loaded for 20 minutes at 37 °C with 1 μM Fura-2 AM (Invitrogen, OR, USA) dissolved in the standard HEK293 cell medium. Excess dye was washed off with HEK293 cell media, and cells were stored in the dark until ready for use. Coverslips were mounted on the stage of an Olympus IX71 inverted microscope (Olympus, Center Valley, PA) equipped with a UAPO 40X objective (NA 1.35). Cells were alternately illuminated at 340 and 380 nm using band-pass filters (Chroma Technology) and the fluorescence emission at 510 nm was captured using a cooled CCD camera (Hamamatsu, Japan), digitized, and analyzed using IPLab software (Sanalytics corp.). The 340 nm/380 nm ratio images were recorded at 6 s intervals.

Western blots. Transfected HEK293 cells (18-24 hr. post-transfection) were treated with 2 μg/ml tunicamycin to reduce glycosylation. Cells were washed with cold PBS and lysed in 150 mM NaCl, 50 mM Tris, 1% Triton-X-100, 0.1% SDS, 1x Protease Inhibitor Cocktail (Sigma). Lysates were spun down at 4°C for 30 min. and supernatants were collected and stored at –20°C. For Western blots, samples were heated to 65°C for 5 min. in Laemmli Sample Buffer (Bio-Rad) containing 0.1% β-mercaptoethanol, run on 10% SDS-PAGE gels, and transferred to nitrocellulose membrane. Orai1 protein was detected using an affinity purified polyclonal antibody (kind gift of Dr. Stefan Feske, NYU) against the C-terminus [10].

FRET microscopy. HEK293 cells were plated onto poly-L-lysine coated coverslip chambers and imaged either with epifluorescence or through-the-objective TIRF microscopy on an IX71 inverted microscope (Olympus, Center Valley, PA). For epifluorescence FRET microscopy, cells

were imaged with a 60x oil immersion objective (UPlanApo NA 1.40), a 175 W Xenon arc lamp (Sutter, Novatao, CA), and excitation and emission filter wheels (Sutter, Novato, CA) as previously described [11]. At each time point, three sets of images (CFP, YFP, and FRET) were captured on a cooled CCD camera (Hamamatsu, Bridgewater, NJ) using optical filters specific for the three images as previously described [12]. Image acquisition and analysis was performed with Slidebook software (Imaging Innovations Inc., Denver, CO). Images were captured at 12 s intervals at an exposure of 200 ms with 2x2 binning. Lamp output was attenuated to 25% by a 0.6 ND filter in the light path to minimize photobleaching. All experiments were performed at room temperature.

FRET analysis was performed using the E-FRET method described by Zal and Gascoigne [13]. Bleedthrough factors (a=0.09; b=0.008; c=0.002 and d=0.33) were determined as previously described [11]. The apparent FRET efficiency was calculated from background-subtracted images using the formalism [13]:

$$E_{app} = \frac{F_c}{F_c + GI_{DD}}$$

where $F_c = I_{DA} - aI_{AA} - dI_{DD}$

I_{DD}, I_{AA} and I_{DA} refer to the background subtracted CFP, YFP, and FRET images, respectively. The instrument dependent *G* factor was determined as described [11] and had the value 2.7±0.2.

TIRF microscopy. HEK293 cells expressing Orai1-CFP and/or STIM1-YFP were illuminated by laser output from an Argon-ion laser (Melles Griot, CA; 457-514 nm output) coupled to an illuminator that focused light on the back focal plane of a TIRF objective (PlanApo 60x, 1.45 NA, Olympus). TIRF illumination was achieved by controlling the position of a translatable

prism to alter the incident angle of the laser beam. CFP and YFP images were collected using the following combinations of filters and dichroics (Chroma): CFP excitation: ET458±10 nm; dichroic: Z458/514RPC; emission: ET485/30; YFP excitation: ET514±10: dichroic: Z458/514RPC; emission: ET550±50. Images were captured with 2x2 pixel binning.

NFAT-luciferase assays. We used NFAT-dependent gene transcription as an indirect readout for constitutive Ca^{2+} influx. An NFAT-dependent luciferase reporter construct described previously [14] was used for these experiments. The construct features three copies of the NFAT binding site linked to a non-inducible minimal IL-2 promoter in the pGL-3 luciferase reporter vector (Promega). To overcome variations in cell density, cell viability, and transfection efficiency, the NFAT driven luciferase activity was normalized to constitutive renilla luciferase activity of the pRL-Tk luciferase vector. HEK293 cells were transfected with the luciferase reporter constructs 24 hours prior to experiments. Cells were stimulated with thapsigargin (0.25 μM) and PDBU (100 nM) for 5 hours, lysed, and assayed for luciferase activity using the Dual Luciferase Reporter Assay kit (Promega) and a single tube luminometer (Berthold Instruments, Germany).

Fractional Ca^{2+} current estimates. HEK293 cells over-expressing V102C Orai1-mCherry alone or WT Orai1-mCherry and unlabeled STIM1 were overloaded with the Ca^{2+} indicator, fluo-4 (1 mM) delivered via the patch pipette. Estimates of the fractional Ca^{2+} current (P_f) in the standard 20 mM Ca^{2+} Ringer's solution were made from changes in the Ca^{2+}-sensitive fluo-4 fluorescence [15]. Cells were held at a holding potential of +50 mV and stepped to -100 mV for 20 s. The amount of charge entering the cell during the voltage pulse was determined from the leak-subtracted integral of CRAC current ($\int I \bullet t$), and the fluorescence-to-charge ratio R was computed

from the relationship $R=\Delta F/\int I \bullet t$. Under the assumption that fluo-4 is not saturated and capturing all of the incoming Ca^{2+}, *R* should be directly proportional to the amount of Ca^{2+} entering the cell [15]. If we assume that the I_{CRAC} from WT Orai1 produces a pure Ca^{2+} current, a direct comparison of *R* between WT Orai1 and V102C Orai1 channels provides an estimate of P_f in V102C Orai1 [15]. It is important to note that P_f is directly influenced by the driving force for Ca^{2+} entry [15], and therefore is predicted to be considerably lower at physiological Ca^{2+} concentrations and membrane potentials than the experimental conditions used here (20 mM Ca^{2+} and -100 mV). We verified that fluo-4 is not saturated under our recording conditions by flooding the cell with 20 mM Ca^{2+} at the end of the experiment.

Estimates of the relative Ca^{2+} permeability. To compare the Ca^{2+} permeability of V102C Orai1 and WT Orai1 channels, we used the extended form of the Goldman-Hodgkin-Katz equation [16] to obtain estimates of their relative Ca^{2+} permeabilities (P_{Ca}/P_{Na}). With Cs^+ as the main internal cation and in the standard Ringer's solution (20 mM Ca^{2+}), the reversal potential of V102C Orai1 I_{CRAC} is 18.1 mV (Supplementary Table 1). Using the modified GHK equations described previously [16,17], and assuming that $P_{Cs}=P_{Na}$ in this mutant (V_{rev} ~ 0 mV in DVF solution), these relations yield a P_{Ca}/P_{Na} value of 6 for V102C Orai1. By contrast, for WT Orai1, the calculated P_{Ca}/P_{Na} is 991 assuming a reversal potential of +80 mV in the standard Ringer's solution (Supplementary Table 1).

Supplementary Figure Legends

Supplementary Figure 1. Blockade of Orai1 Cys mutants by extracellularly applied MTSEA. a, Rapid blockade of G98C by MTSEA in DVF solution. MTSEA (100 μM) was applied in DVF solution to a cell expressing G98C E106D Orai1 together with STIM1. Arrows indicate the time points at which the current amplitudes were measured. The *right* graph shows a summary of the reaction rate constants of MTSEA blockade in the standard Ringer's solution (20 mM Ca^{2+}) and DVF solution. **b,** Blockade of G98C E106D Orai1 currents by extracellularly applied MTSEA (100 μM) is unaffected by inclusion of a thiol scavenger, L-cysteine (10 mM) in the patch-pipette. Because MTSEA is partially membrane permeable [18], this result indicates that MTSEA inhibition does not result from effects in the intracellular side of the membrane. The bar graph shows the degree of MTSEA inhibition (mean±SEM; n=4-6) in cells with and without L-cysteine. **c,** MTSEA blocks V102C E106D Orai1 currents. Application of MTSEA (200 μM) in DVF solution results in inhibition of V102C E106D Orai1 currents. Although both the monovalent and Ca^{2+} currents are inhibited, the graph is shown at a high gain to illustrate the persistent inhibition of the Ca^{2+} current. The bar graph summarizes the blockade (mean±SEM) by MTSEA in the indicated mutant. **d,** MTSET (200 μM) does not inhibit G98C E106D currents. MTSET is a larger analogue of MTSEA (5.8 vs. 3.8 Å), suggesting that although enlarged, the E106D pore is still sufficiently narrow to prevent access of MTSET. The bar graph on the right summarizes the effects (mean±SEM) of MTSEA and MTSET in G98C E106D Orai1 channels.

Supplementary Figure 2. V102C Orai1 channels are constitutively active. a, Intracellular $[Ca^{2+}]_i$ measured with fura-2 in HEK293 cells transfected with the indicated Orai1 constructs together with STIM1. Cells transfected with V102C Orai1 exhibit high levels of resting $[Ca^{2+}]_i$, which is strongly diminished by removing extracellular Ca^{2+}, indicating constitutive Ca^{2+} entry. **b,** Resting cells expressing V102C Orai1 and STIM1 exhibit constitutive induction of NFAT-dependent luciferase expression. Note that the thapsigargin-induced luciferase activity is significantly larger than the gene expression induced by constitutive activity of V102C Orai1, indicating that activation of STIM1 elicits a much higher level of NFAT-dependent gene expression than that afforded by constitutive activity of V102C Orai1. **c,** Constitutive induction of NFAT-dependent luciferase activity in cells expressing V102C Orai1 alone.

Supplementary Figure 3. The constitutively active V102C Orai1 channels fail to show CDI in the absence of STIM1. In each case, traces represent currents elicited by hyperpolarizing voltage steps (300 ms) to -100 mV. Co-expression of STIM1 restores CDI of V102C Orai1 channels. To accentuate the extent and rate of CDI and eliminate potential confounding effects of Na^+ permeation in STIM1-free V102C Orai1 channels, these experiments were performed in 110 mM Ca^{2+} and with intracellular EGTA (instead of BAPTA).

Supplementary Figure 4. V102C L276D Orai1 channels fail to interact with STIM1. a, E-FRET measurements showing increases in FRET between the indicated Orai1-CFP mutants and STIM1-YFP. Interaction of V102C Orai1 with STIM1 is indistinguishable from that of WT Orai1, indicating that the mutation does not detectably alter STIM1-Orai1 binding. **b,** By contrast, the V102C L276D Orai1 double mutant fails to interact with STIM1. **c**, Summary of the

resting E-FRET and changes in E-FRET (mean±SEM) in response to store depletion with 1 μM thapsigargin in the indicated mutants.

Supplementary Figure 5. Mutational analysis of the constitutive activation phenotype. a, The constitutive activation phenotype of V102C is not observed in Cys mutations at the TM1 Orai1 pore-lining positions, L95 and G98, and is diminished by the loss of function mutations, E106A and R91W [17,19]. Example recordings from cells expressing the indicated Orai1 mutants expressed alone (i.e., no STIM1). The bar graph on the *right* summarizes the mean currents (±SEM) in the indicated mutants. **(b)** The size of the side-chain at V102 influences the degree of constitutive and STIM1-gated CRAC channel activity. *Left graph*, the current density of different V102 mutants (without STIM1) was plotted against the amino acid side-chain surface area. All currents were normalized to the maximal current density seen in the Ala mutant. *Right graph*, the normalized current density of hydrophobic V102 mutants (with STIM1) was plotted against side-chain surface area. Although hydrophobic residues (I, V, L, and M) exhibited STIM1-gating (but not constitutive activation), the introduction of large hydrophobic residues (F, W), resulted in non-functional channels both in the presence and absence of STIM1. Substitutions producing constitutive activation are depicted in red.

Supplementary Figure 6. Mutation of V77 in Orai3 produces constitutively open Orai3 channels with altered ion selectivity. a, Current at -100 mV in a HEK293 cell transfected with V77C CFP-Orai3 and STIM1. The right graphs illustrate the I-V relationships of the current in 20 mM Ca^{2+} and DVF solutions. **b,** Constitutive activity of V77C Orai3 channels in the absence of STIM1-co-expression. In each case, the cell was transfected with either WT CFP-Orai3 alone or V77C CFP-Orai3 alone (no STIM1). The I-V relationship of the current is depicted in the *right* plots. In contrast to WT Orai3 channels, the V77C Orai3 channels produce large, constitutively active currents. **c,** Reversal potentials (mean±SEM) of V77C CFP-Orai3 currents in 20 mM Ca^{2+} and DVF solutions in the presence and absence of STIM1 co-expression.

Supplementary Figure 7. STIM1 regulates Ca^{2+}, Sr^{2+} and Ba^{2+} permeation in V102C Orai1 channels. (a) Fractional Ca^{2+} current measurements in V102C Orai1 channels. Example of flou-4 fluorescence and inward current in 20 mM Ca^{2+} Ringer's solution in a cell expressing V102C Orai1-mCherry. 1 mM fluo-4 was introduced into the cell via the patch pipette. The cell was held at a holding potential of +50 mV and stepped briefly to -100 mV (20 s) to elicit Ca^{2+} influx. The right plot summarizes the ratio *R* of the increase in fluorescence signal over the current integral during the hyperpolarizing pulse ($R=\Delta F/\int I \bullet t$). Assuming that WT Orai1 channels conduct only Ca^{2+}, a direct comparison of *R* values in WT and V102C Orai1 provides an estimate of the fractional Ca^{2+} current (P_f) in V102C Orai1 channels [15]. **(b)** Ba^{2+} and Sr^{2+} permeation. Currents resulting from substitution of extracellular Ca^{2+} with equimolar concentrations of either Sr^{2+} or Ba^{2+} in the presence or absence of STIM1 co-expression. In the presence of STIM1, equimolar substitution of Ca^{2+} with Sr^{2+} or Ba^{2+} results in enlarged currents that slowly decline over tens of

seconds due to depotentiation. However, in the absence of STIM1, Ba^{2+} and Sr^{2+} currents are significantly smaller, suggesting that STIM1 regulates permeation of these divalent ions.

Supplementary Figure 8. Analysis of Cd^{2+} block suggests that the subunit stoichiometry of the constitutively active V102 channels is similar in the presence and absence of STIM1.

a, Schematic of the concatenated tandem dimer constructs used for analyzing subunit stoichiometry. Constitutive activation was achieved by introducing the V102A mutation in both protomers. Cd^{2+} sensitivity was conferred by introducing the D110C mutation in either one, or both protomers of the dimer. Tetrameric channels containing either two or four pore-lining cysteines at D110 were obtained by co-expressing the concatemers with STIM1. The bar graph on the right summarizes the degree of Cd^{2+} block (mean±SEM) in the indicated constructs, in the presence or absence of STIM. In the STIM1-free V102A dimer containing D110C substitutions in both protomers, Cd^{2+} block is similar in the absence and presence of STIM1. Moreover, in the absence of STIM1, Cd^{2+} block in this dimer is significantly greater than block in dimers with only one D110C-bearing subunit in the presence of STIM1, implying that there must be > 2 pore-lining Cys in the STIM1-free V102A channels. **b**, Western blots showing expression of Orai1 tandem constructs. The blots show monomeric and dimeric Orai1 constructs, along with V102A dimers with D110C on one or both protomers. Multiple bands may reflect incomplete removal of glycosylation by tunicamycin. **c,** Cd^{2+} blockade of constitutively active monomeric and dimeric V102A D110C Orai1 mutants in the absence or presence of STIM1. In all cases, Cd^{2+} block is largely irreversible, indicating that the ion is trapped in the pore presumably due to tight coordination of Cd^{2+} by Cys side-chains [5]. Recovery from Cd^{2+} blockade required perfusion of BMS to destabilize Cd^{2+} coordination, consistent with Cd^{2+} trapping in the pore.

Supplementary Figure 9. STIM1 modulates CDI and ion selectivity of Orai1 channels. a, Example traces showing currents during hyperpolarizing steps to -100 mV in HEK293 cells expressing the indicated Orai1 constructs. CDI is not detectable in Orai1-S constructs, but is readily apparent in Orai1-SS constructs, indicating that increasing the local STIM1 concentration enhances Orai1 CDI, consistent with recent findings [20]. **b**, The ion selectivity of Orai1 depends on the STIM1: Orai1 ratio. Full-length STIM1 and WT Orai1 were co-expressed at the indicated ratios. Substitution of extracellular Na^+ with an impermeant ion, $NMDG^+$, diminishes the inward current at low STIM1:Orai1 ratios, indicating that Orai1 channels conduct Na^+. This is not observed when the STIM1:Orai1 ratio is high. The *right* graphs show the I-V relationships of currents in 2 mM Ca and divalent-free (DVF) Ringer's solutions, and reveal that when STIM1 is limiting, Orai1 channels display diminished permeability to Ca^{2+} and increased permeability to intracellular Cs^+. V_{rev} in the DVF solution shifts from ~+50 mV when STIM1 is high to ~0 mV when STIM1 is low, indicating that an excess of STIM1 diminishes CRAC channel permeability to Cs^+. As previously reported [20,21], I_{CRAC} at the 1:4 STIM1:Orai1 ratio did not display CDI, in contrast to high the 10:1 STIM1:Orai1 ratio where CDI was clearly observed (data not shown).

Supplementary References

1 McNally, B. A., Yamashita, M., Engh, A. & Prakriya, M. Structural determinants of ion permeation in CRAC channels. *Proc Natl Acad Sci U S A* **106**, 22516-22521 (2009).

2 Stauffer, D. A. & Karlin, A. Electrostatic potential of the acetylcholine binding sites in the nicotinic receptor probed by reactions of binding-site cysteines with charged methanethiosulfonates. *Biochemistry* **33**, 6840-6849 (1994).

3 Prakriya, M. & Lewis, R. S. Regulation of CRAC channel activity by recruitment of silent channels to a high open-probability gating mode. *J. Gen. Physiol* **128**, 373-386 (2006).

4 Penna, A. *et al.* The CRAC channel consists of a tetramer formed by Stim-induced dimerization of Orai dimers. *Nature* **456**, 116-120 (2008).

5 Liu, Y., Holmgren, M., Jurman, M. E. & Yellen, G. Gated access to the pore of a voltage-dependent K^+ channel. *Neuron* **19**, 175-184 (1997).

6 Loussouarn, G., Phillips, L. R., Masia, R., Rose, T. & Nichols, C. G. Flexibility of the Kir6.2 inward rectifier K^+ channel pore. *Proc Natl Acad Sci U S A* **98**, 4227-4232 (2001).

7 Mignen, O., Thompson, J. L. & Shuttleworth, T. J. Orai1 subunit stoichiometry of the mammalian CRAC channel pore. *J Physiol* **586**, 419-425 (2008).

8 Madl, J. *et al.* Resting-state Orai1 diffuses as homotetramer in the plasma membrane of live mammalian cells. *J Biol Chem* **285**, 41135-41142 (2010).

9 Srikanth, S., Yee, M. K., Gwack, Y. & Ribalet, B. The third transmembrane segment of orai1 protein modulates Ca^{2+} release-activated Ca^{2+} (CRAC) channel gating and permeation properties. *J Biol Chem* **286**, 35318-35328 (2011).

10 Gwack, Y. *et al.* Hair loss and defective T- and B-cell function in mice lacking ORAI1. *Mol Cell Biol* **28**, 5209-5222 (2008).

11 Navarro-Borelly, L. *et al.* STIM1-Orai1 interactions and Orai1 conformational changes revealed by live-cell FRET microscopy. *J Physiol* **586**, 5383-5401 (2008).

12 Yamashita, M., Somasundaram, A. & Prakriya, M. Competitive modulation of CRAC channel gating by STIM1 and 2-aminoethyldiphenyl borate (2-APB). *J Biol Chem* **286**, 9429-9442 (2011).

13 Zal, T. & Gascoigne, N. R. Photobleaching-corrected FRET efficiency imaging of live cells. *Biophys J* **86**, 3923-3939 (2004).

14 Mattila, P. S. *et al.* The actions of cyclosporin A and FK506 suggest a novel step in the activation of T lymphocytes. *Embo J* **9**, 4425-4433 (1990).

15 Neher, E. The use of fura-2 for estimating Ca buffers and Ca fluxes. *Neuropharmacology* **34**, 1423-1442 (1995).

16 Jan, L. Y. & Jan, Y. N. L-glutamate as an excitatory transmitter at the Drosophila larval neuromuscular junction. *J Physiol* **262**, 215-236 (1976).

17 Prakriya, M. *et al.* Orai1 is an essential pore subunit of the CRAC channel. *Nature* **443**, 230-233 (2006).

18 Holmgren, M., Liu, Y., Xu, Y. & Yellen, G. On the use of thiol-modifying agents to determine channel topology. *Neuropharmacology* **35**, 797-804 (1996).

19 Feske, S. *et al.* A mutation in Orai1 causes immune deficiency by abrogating CRAC channel function. *Nature* **441**, 179-185 (2006).

20 Hoover, P. J. & Lewis, R. S. Stoichiometric requirements for trapping and gating of Ca^{2+} release-activated Ca^{2+} (CRAC) channels by stromal interaction molecule 1 (STIM1). *Proc Natl Acad Sci U S A* **108**, 13299-13304 (2011).

21 Scrimgeour, N., Litjens, T., Ma, L., Barritt, G. J. & Rychkov, G. Y. Properties of Orai1 mediated store-operated current depend on the expression levels of STIM1 and Orai1 proteins. *J Physiol* (2009).

Supplementary Table 1. Properties of Orai1 mutants

Construct	with STIM1			without STIM1		
	Current Density (I(pA/pF) ± SEM)	Reversal Potential (mV ± SEM)		Current Density (I(pA)/pF) ± SEM)	Reversal Potential (mV ± SEM)	
		20 Ca	DVF		20 Ca	DVF
WT O1	-38.7 ± 6.9	> 80	43.3 ± 3.3	-0.105 ± 0.046	--	--
V102C	-24.1± 3.4	74.6 ± 2.3	49.6 ± 1.7	-45.1± 6.2	18.3 ± 1.4	3.05 ± 0.45
V102C siSTIM1				-27.4± 6.6	19.4 ± 2.3	5.9 ± 2.2
V102L	-30.4 ± 0.87	66.7 ± 3.8	37.3 ± 5.2	-0.007 ± 0.002	--	--
V102I	-71.2 ± 9.4	52 ± 2.8	48.0 ± 2.6	-0.162 ± 0.029	--	--
V102P	-1.08 ± 0.420	--	--	-0.236 ± 0.125	--	--
V102F	-0.438 ± 0.095	--	--	-0.0879 ± 0.031	--	--
V102M	-51.4 ± 8.5	68.7 ± 1.2	47.0 ± 2.1	-3.91 ± 1.045	--	--
V102W	-0.276 ± 0.046	--	--	-0.027 ± 0.011	--	--
V102A	-23.6 ± 8.0	61.7 ± 6.0	48.2 ± 1.3	-112.1 ± 16.9	21.5 ± 3.3	5.84 ± 1.66
V102G	-41.4 ± 21.8	38.2 ± 3.8	41.4 ± 2.4	-74.8 ± 25.1	16.7 ± 2.4	14.6 ± 1.6
V102Y	-0.583 ± 0.10	--	--	-0.188 ± 0.093	---	---
V102T	-3.65 ± 0.52	62.5 ± 2.5	53.0 ± 4.8	-32.4 ± 5.0	19.0 ± 1.3	2.9 ± 2.4
V102S	-10.5 ± 4.9	60.0 ± 3.2	46.5 ± 4.0	-24.3 ± 5.7	21.4 ± 4.6	25.0 ± 5.0
V102H	-3.50 ± 1.048	--	--	-3.97 ± 1.131	---	---
V102Q	-14.9 ± 3.5	11.8 ± 6.3	33.4 ± 3.1	-8.23 ± 2.06	6.44 ± 2.36	14.3 ± 4.6
V102K	-1.00 ± 0.34	--	--	-5.45 ± 2.14	0.69 ± 2.07	8.9 ± 1.5
V102N	-2.67 ± 0.39	--	--	-2.03 ± 1.04	--	--
V102E	-1.35 ± 0.70	--	--	-0.292 ± 0.165	--	--
V102D	-0.626 ± 0.27	--	--	-1.35 ± 0.70	--	--
V102R	-0.740 ± 0.31	--	--	-4.75 ± 1.34	--	--
L95C				-0.113 ± 0.016	--	--
G98C				-0.17 ± 0.05	--	--
CFP V77C O3	-66.3 ± 19.7	24 ± 3.2	34.7 ± 2.9	-42.5 ± 6.0	17.6 ± 3.8	-4.0 ± 2.7
Orai1-S				-3.93 ± 0.43	32.1 ± 1.2	8.3 ± 1.9
Orai1-SS				-15.3 ± 2.1	66.2 ± 5.6	44.1 ± 2.3
V102C-S				-19.8 ± 2.9	30.6 ± 2.6	24.1 ± 2.9
V102C-SS				-28.9 ± 8.9	50.2 ± 10.8	49.2 ± 2.9

Currents were measured in mutants generated in the WT Orai1 or CFP Orai3 background. Reversal potentials determined from ramps (-100 to 100 mV) and current densities measured at -100 mV are shown as mean ± SEM; *n*= 4–13 cells. "--" denotes reversal potentials that could not be reliably determined from cells with current densities less than 5 pA/pF.

Supplementary Figure 1

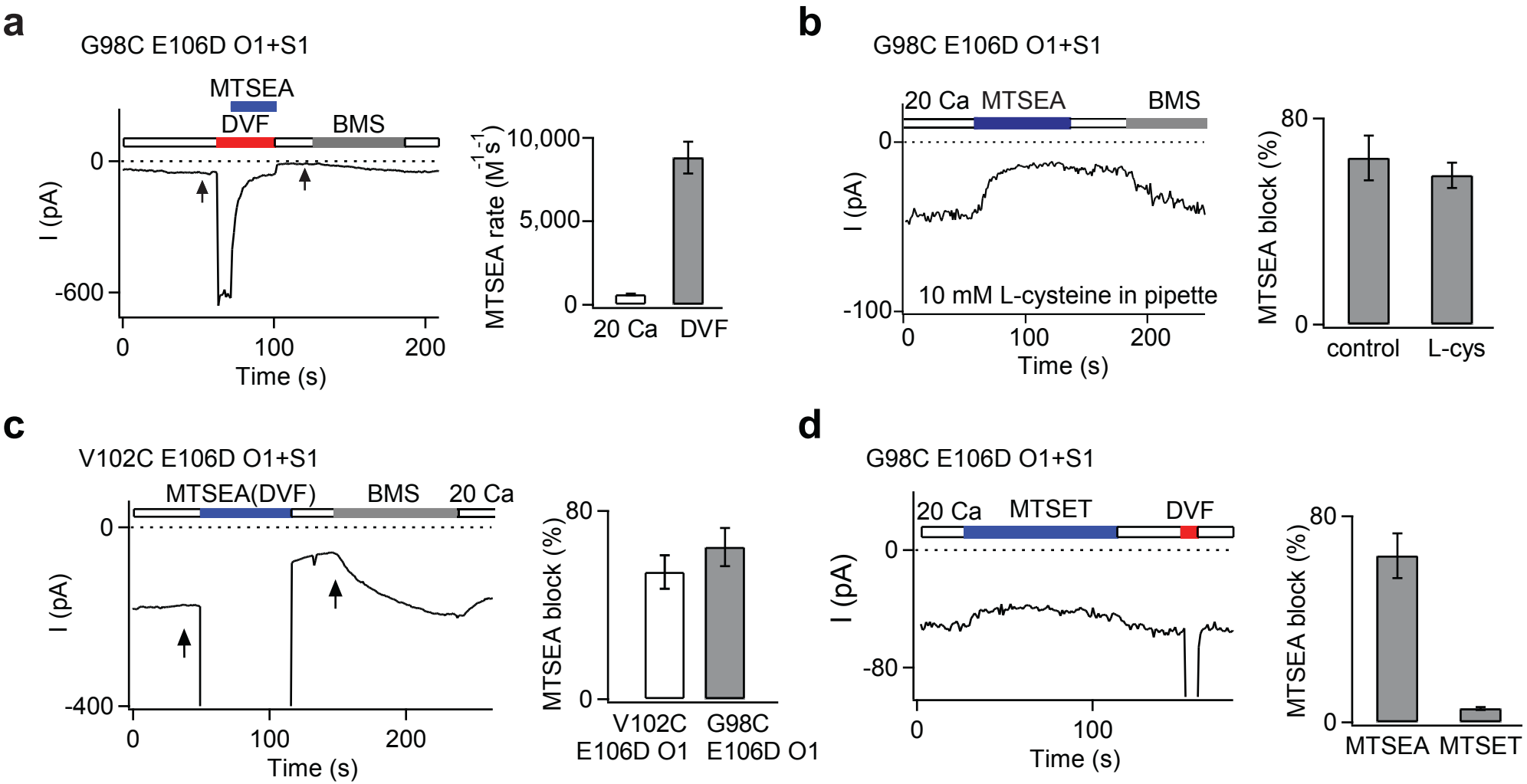

Supplementary Figure 2

a

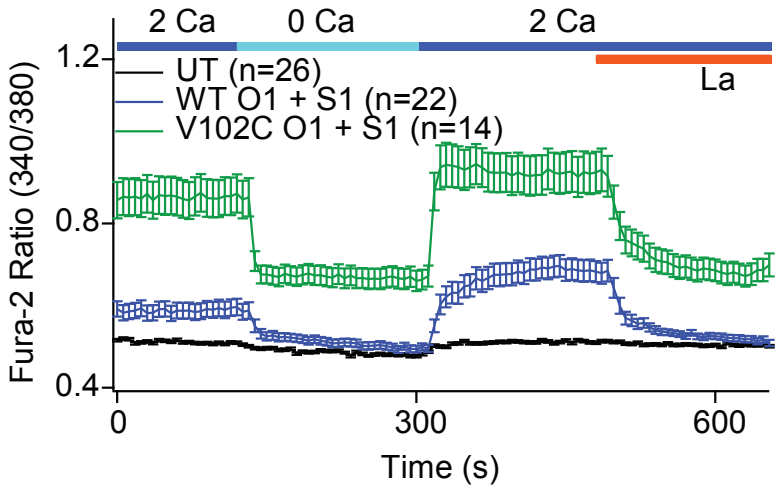

b

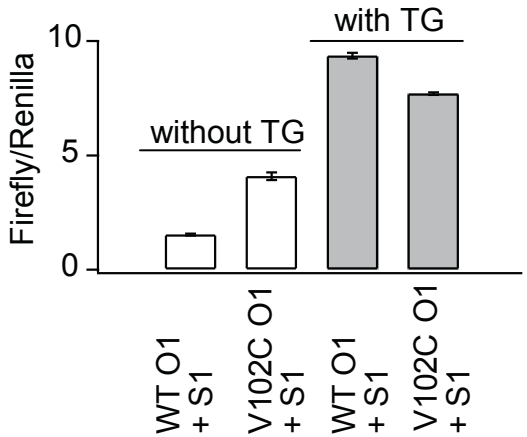

c

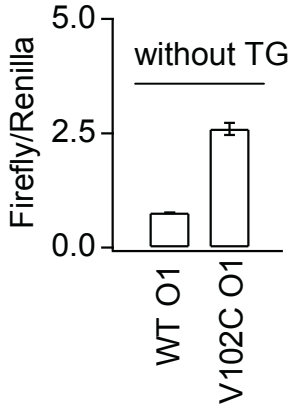

Supplementary Figure 3

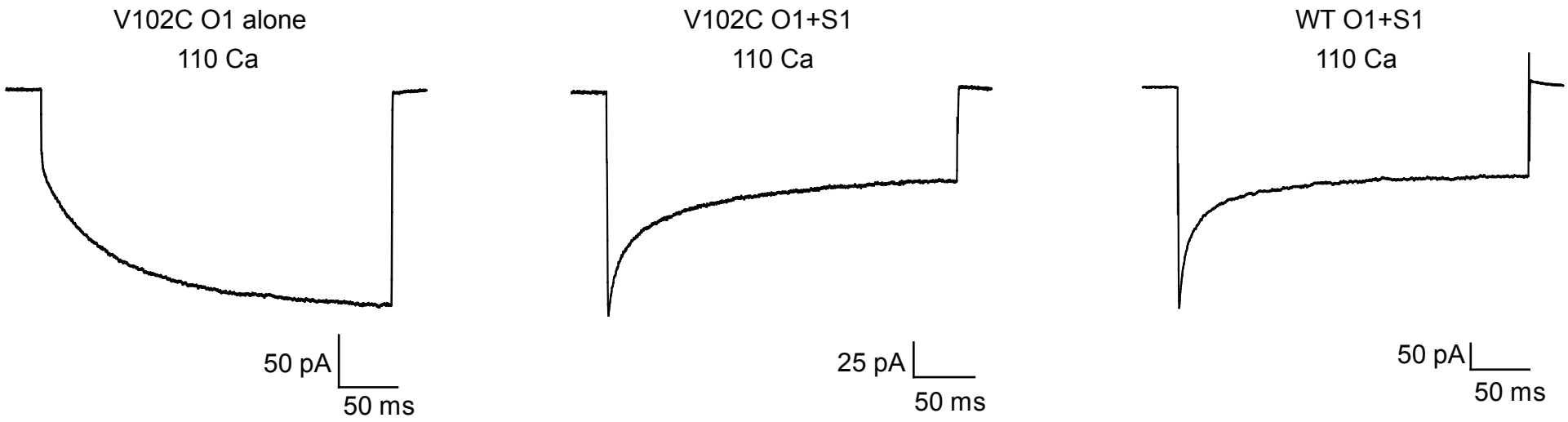

Supplementary Figure 4

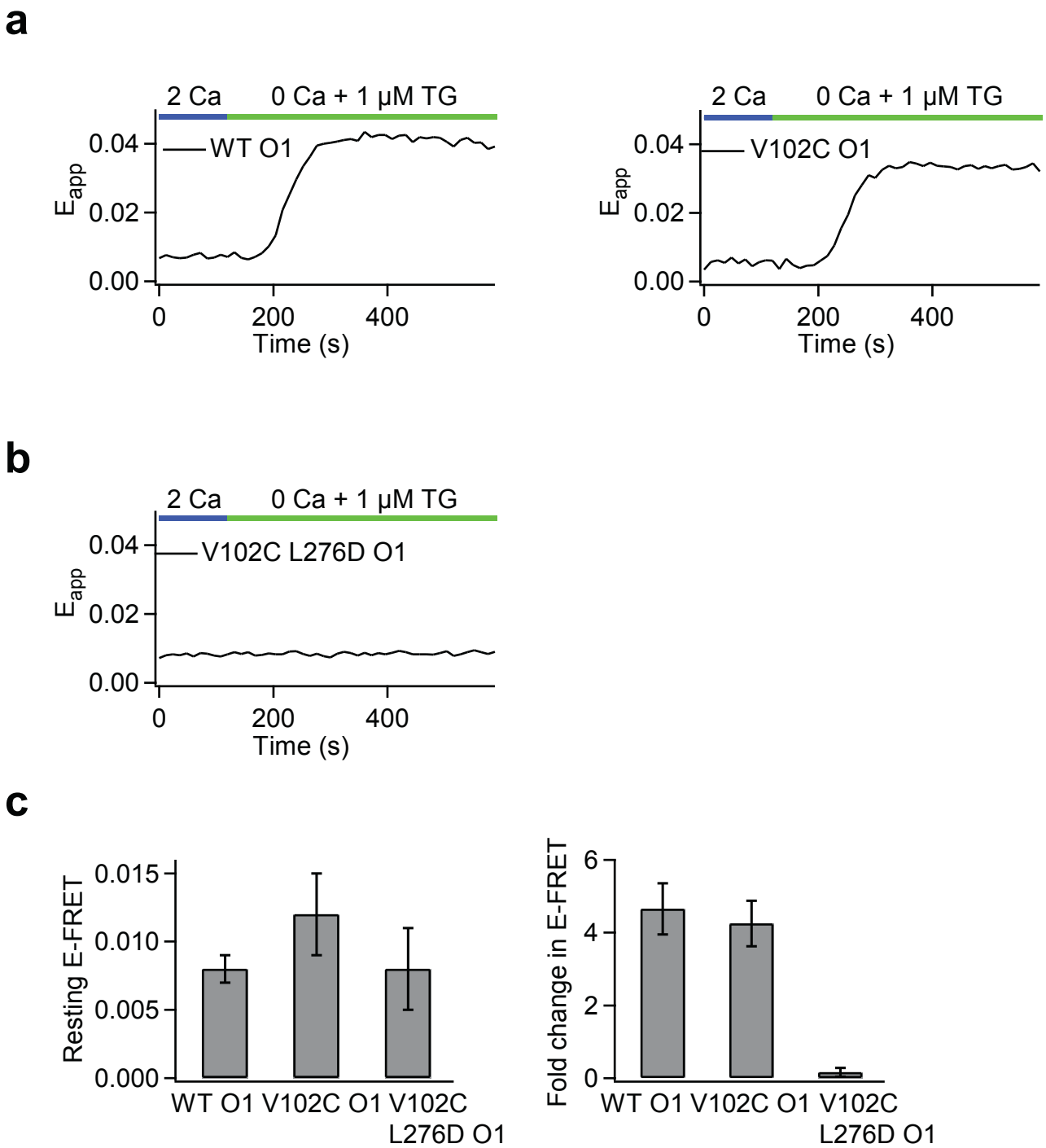

Supplementary Figure 5

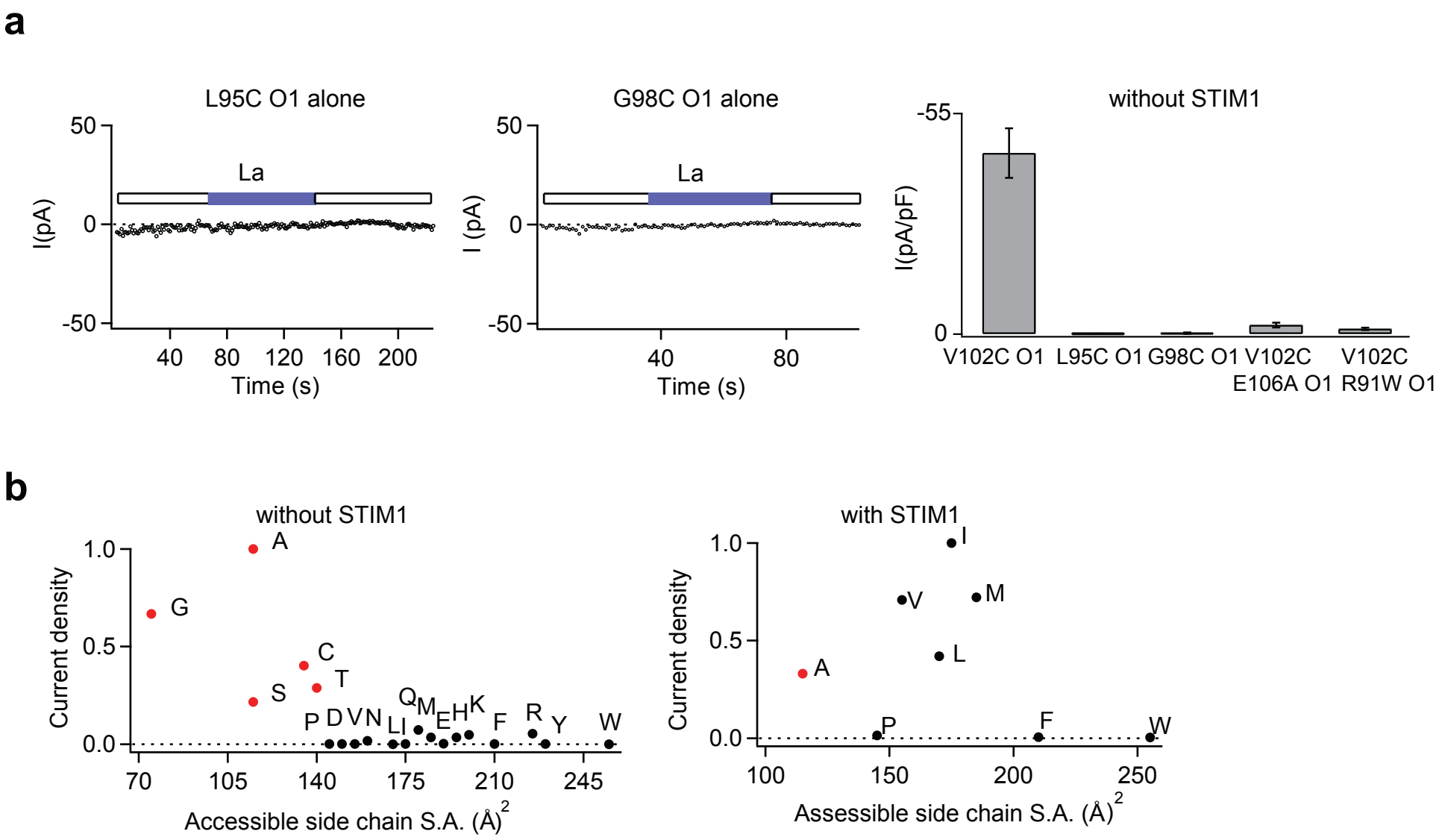

Supplementary Figure 6

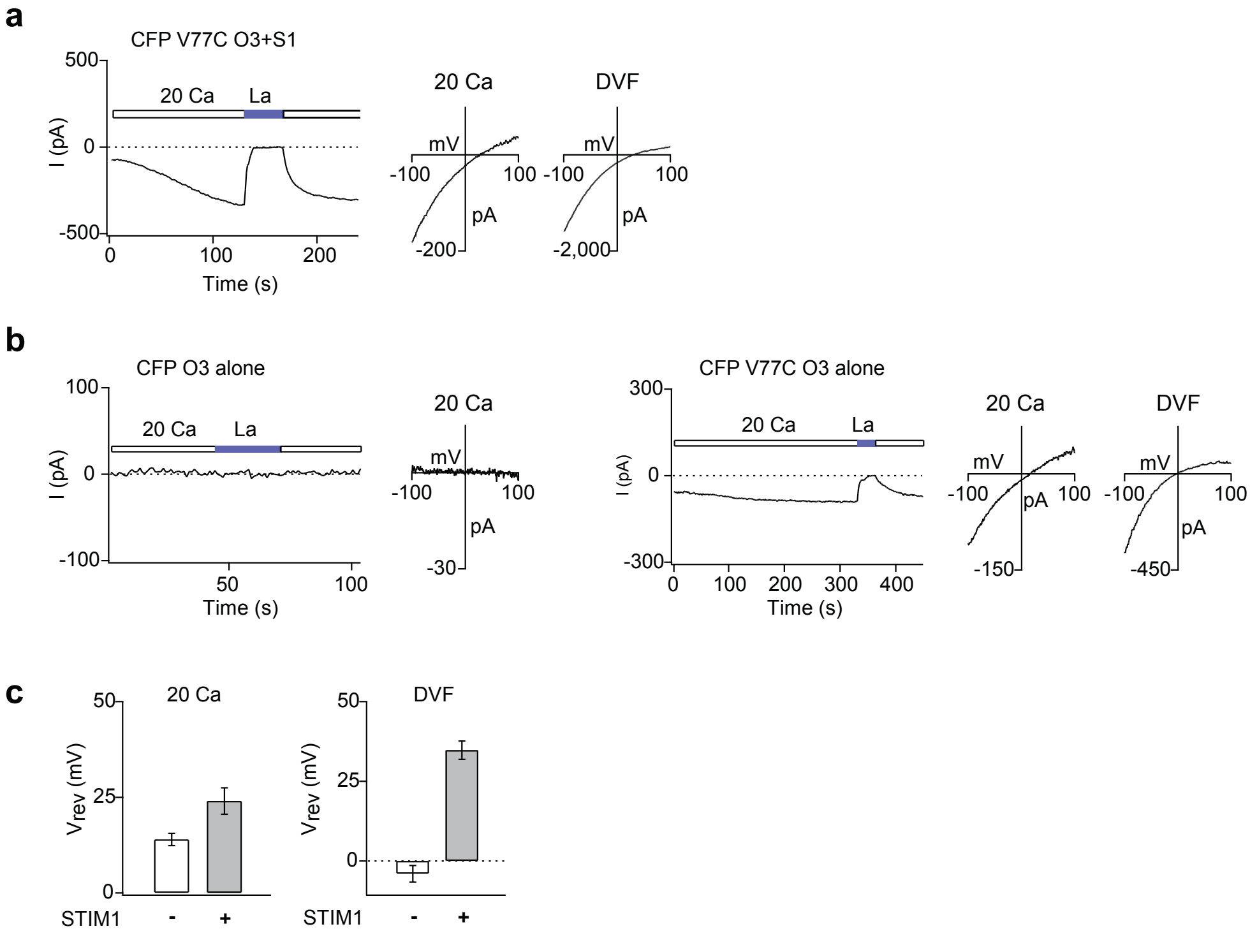

Supplementary Figure 7

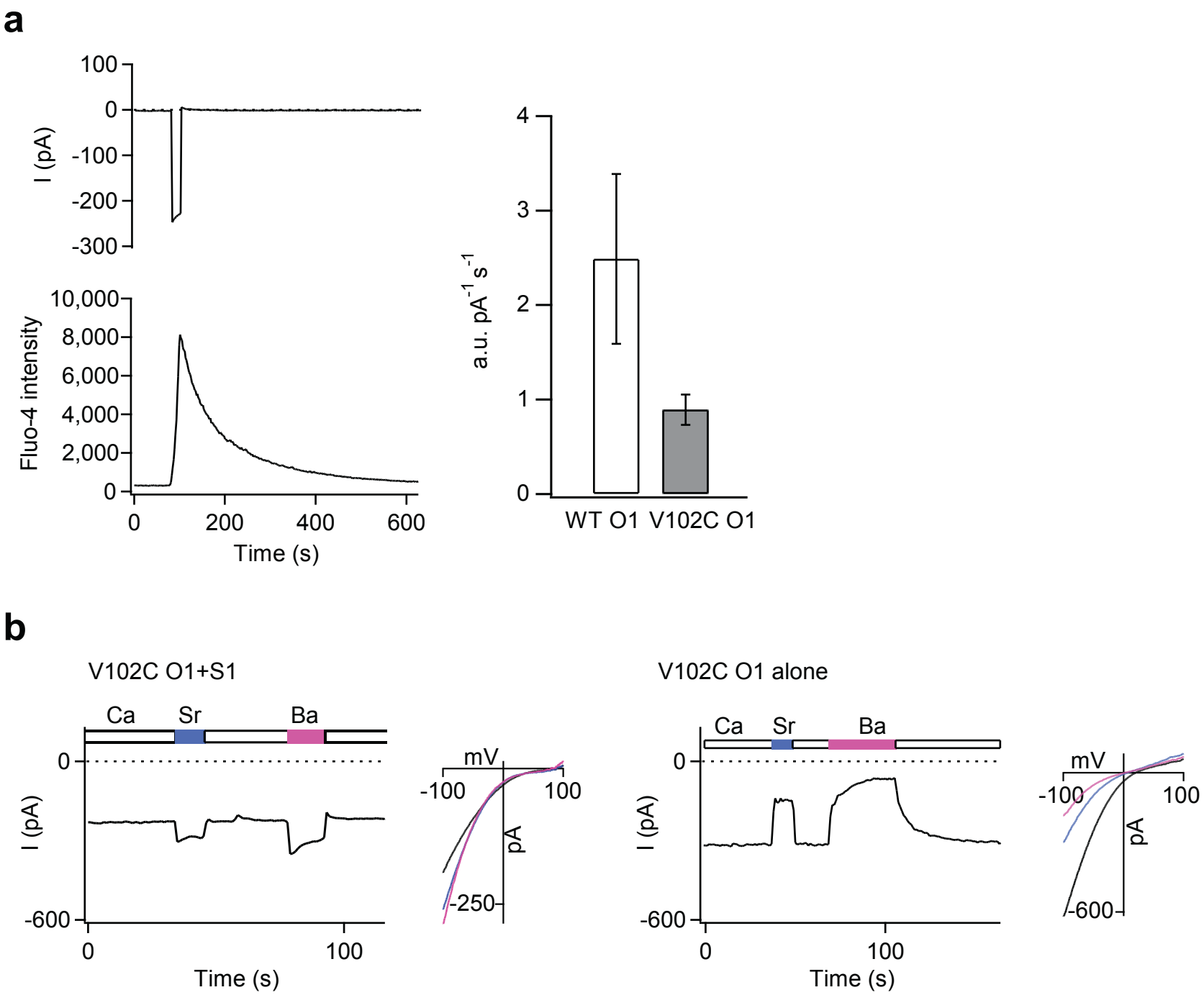

Supplementary Figure 8

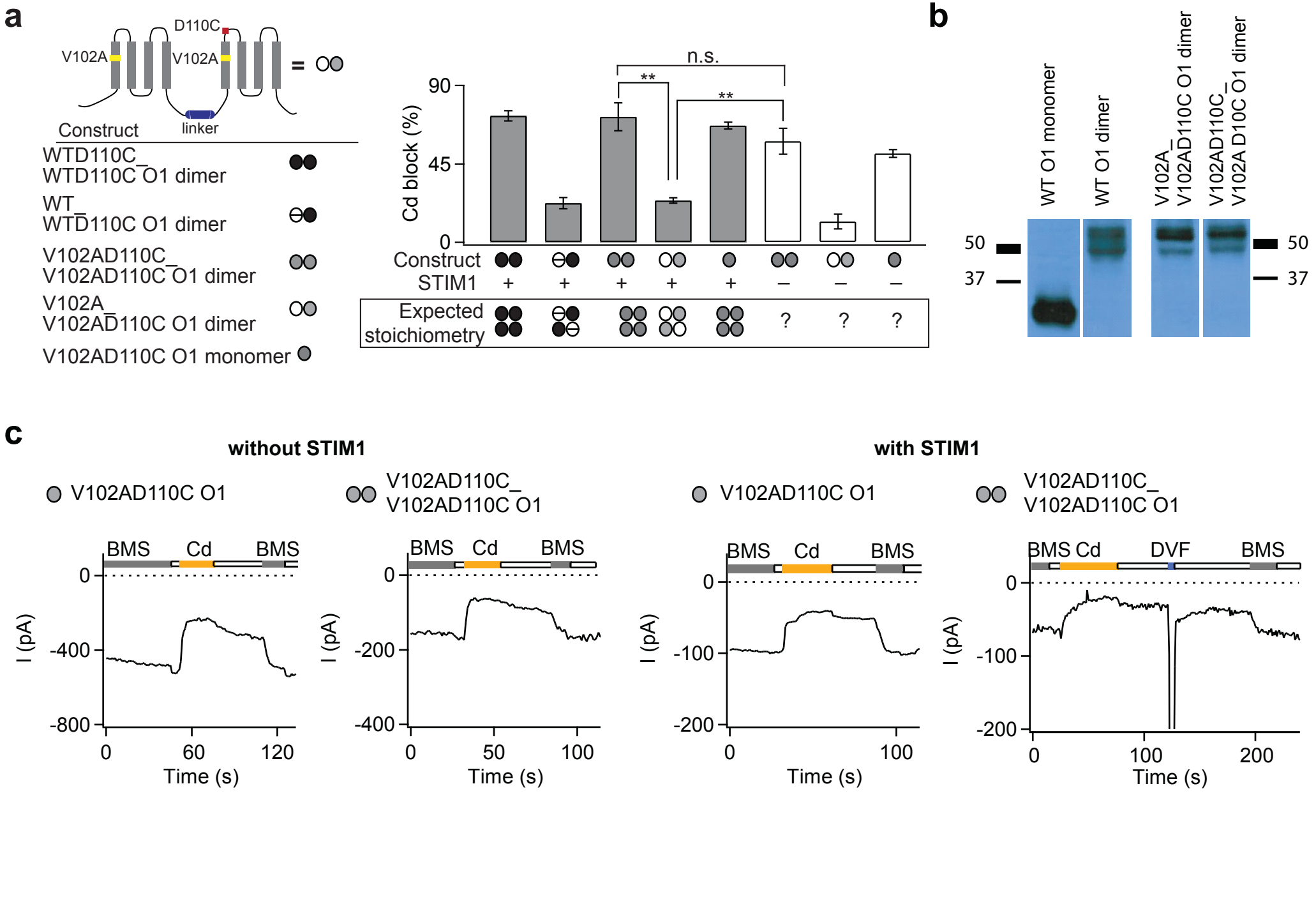

Supplementary Figure 9